Supporting Information for "Sediments in sea ice drive the Canada Basin surface Mn maximum: insights from an Arctic Mn ocean model"

B. Rogalla[1], S. E. Allen[1], M. Colombo[1], P. G. Myers[2], K. J. Orians[1]

[1]Department of Earth, Ocean, and Atmospheric Sciences, University of British Columbia, Vancouver, British Columbia V6T1Z4, Canada

[2]Department of Earth and Atmospheric Sciences, University of Alberta, 1-26 ESB, Edmonton, Alberta T6G2E3, Canada

Contents of this file

1. Text S1 to S4
2. Figures S1 to S19
3. Table S1 to S2

Corresponding author: B. Rogalla, Department of Earth, Ocean, and Atmospheric Sciences, University of British Columbia, Earth Sciences Building, Vancouver BC V6T1Z4, Canada. (brogalla@eoas.ubc.ca)

Text S1. Model boundary condition sensitivity experiments.

The Arctic Mn model domain has three boundaries: the western boundary extends along the Beaufort shelf and the western Canada Basin, the northern boundary extends along northern Canada Basin to Greenland, and the eastern boundary crosses Baffin Bay (Fig. 1). We conducted sensitivity experiments for the western and northern boundary condition, as these regions are most important to the key findings of this study. These sensitivity experiments were spun-up for three years, as for the other experiments, and then run from 2002-2005. By 2005, the year-to-year variations in the the extent of influence of the altered boundary concentrations is small and differences are related to specific flow conditions for that year.

Pacific water enters the Arctic Ocean through Bering Strait and is transported eastward along the North American continent by the Alaskan Coastal current. In the context of our Mn model domain, the Pacific water inflow occurs along the western model boundary. We conducted an experiment with artificially enhanced concentrations along the Beaufort Shelf in the western boundary condition to identify the extent of influence of the Pacific water (Fig. S1); the "Pacific water" experiment. Polar mixed layer dissolved Mn concentrations in September, 2005 are higher over the Beaufort shelf in the Pacific water experiment (Fig. S2). The influence of the increased western boundary dMn contribution is primarily restricted to the Beaufort shelf and minimally impacts the central Canada Basin. A weak increase in concentrations extends along the Chukchi borderland from the northern section of the western boundary condition.

The model northern boundary extends across northern Canada Basin to Greenland. In the context of our Mn model domain, the central Arctic Ocean or transpolar drift inflow

occurs along the northern model boundary. In order to assess the impact of the transpolar drift content on the interior of the Canada Basin, we conducted an experiment with concentrations artificially enhanced along the the northern boundary condition (Fig. S3), in particular towards Ellesmere Island where southward flow occurs; the "transpolar drift" experiment. An increase in dissolved Mn of 2-3 nM at the northern boundary results in an increase of around 0.4 nM near the boundary and less than 0.1 nM in the interior of the Canada Basin by September, 2005 (Fig. S4). Nares Strait sees an increase in dMn concentrations of 0.3-0.5 nM; indicative of the direct transport of waters from the central Arctic Ocean through Nares Strait.

Text S2. Reversible Scavenging parameterization details.

Dissolved Mn adsorbs to particle surfaces (pMn) and oxidises to oMn forming larger aggregates which sink. dMn is regenerated through the release of Mn from particles through desorption and by the reduction of oMn. These processes constitute the reversible scavenging of Mn and can be represented as follows (expanded from Van Hulten et al., 2017):

$$\frac{\partial[dMn]}{\partial t} = -k_{ox} \cdot [dMn] + k_{re} \cdot [oMn] - k_{ad} \cdot [dMn] + k_{de} \cdot [pMn] + \text{physics} + \text{S} \quad (1)$$

$$\frac{\partial[pMn]}{\partial t} = k_{ad} \cdot [dMn] - k_{de} \cdot [pMn] - s_p \frac{\partial[pMn]}{\partial z} + \text{physics} + \text{S} \quad (2)$$

$$\frac{\partial[oMn]}{\partial t} = k_{ox} \cdot [dMn] - k_{re} \cdot [oMn] - s_{ox} \frac{\partial[oMn]}{\partial z} + \text{physics} \quad (3)$$

where s_p and s_{ox} are the pMn and oMn sinking rates, respectively, and k_{ad}, k_{ox}, k_{de}, and k_{re} are the rate constants for adsorption, oxidation, desorption, and reduction. In our model, we trace dMn and oMn explicitly, while we only take the indirect effect of particle-bound Mn on dissolved Mn concentrations into account.

The physics term represents mixing and advection processes, and S represents the contribution from sources and sinks. Away from sources and sinks, assuming steady state, negligible impact of mixing and advection, and a weak vertical gradient in Mn concentrations, the equations are decoupled and we can estimate the scavenging rates from Eqn. 2 and 3:

$$[dMn] = \frac{k_{re}}{k_{ox}} \cdot [oMn] \quad (4)$$

$$[dMn] = \frac{k_{de}}{k_{ad}} \cdot [pMn] \quad (5)$$

Using the ratio of observed dissolved and oxidized (Eqn. 4) or particulate Mn (Eqn. 5) concentrations in the Canadian Arctic (Colombo et al., 2020, 2022), we can estimate

the background scavenging rates for oxidation or adsorption, $k_p = k_{ox}$ or k_{ad}, and for reduction or desorption, $k_d = k_{de}$ or k_{re}, respectively. We consider only observations in regions far away from coastal processes and the ocean surface where the assumptions hold. This condition reduces the available observations to those from stations in deeper areas of Baffin Bay and Canada Basin (Fig. S8) which have relatively small particle fluxes and are far away from sources. We match observations of dissolved and oxidized or particulate Mn at equal depths and fit a linear regression through the origin (Fig. S9). Using this method, the ratio of scavenging rates, k_p/k_d, is estimated to be 1.47 ± 0.25 (uncertainty estimate is the root-mean-square error) and with a k_d of $4.7 \cdot 10^{-7}$ s^{-1} (Bruland et al., 1994), k_p is estimated as $7.0 \cdot 10^{-7}$ s^{-1}.

Since we model dMn and oMn, the final reversible scavenging equations in our Mn model are:

$$\frac{\partial[dMn]}{\partial t} = -k_p \cdot [dMn] + k_d \cdot [oMn] + \text{physics} + \text{S} \tag{6}$$

$$\frac{\partial[oMn]}{\partial t} = k_p \cdot [dMn] - k_d \cdot [oMn] - s_{ox}\frac{\partial[oMn]}{\partial z} + \text{physics} \tag{7}$$

These equations do not incorporate a dependence on the dissolved oxygen concentration since Arctic waters are generally well oxygenated.

Text S3. Comparison of estimate of magnitude of biological uptake.

We estimate that uptake can account for a difference in Mn concentrations of up to about 0.3 nM (Fig. S19). In order to assess our estimate, we can compare the nitrogen uptake from our model forcing with that estimated from observed primary production in the CAA.

Michel, Ingram, and Harris (2006) estimate primary production in the CAA as 53-57 MtC yr^{-1}. Using the average, 55 MtC yr^{-1}, and an area of $2.5{\cdot}10^6$ km^2 for the CAA, this primary production corresponds to 22 gC m^{-2} yr^{-1}. Taking into account the molecular weight of carbon (12 g mol^{-1}) and the Redfield ratio (106C : 16N), primary production accounts for an uptake of 0.28 moles of N m^{-2} yr^{-1}. Our estimate of uptake from the CanOE model is on the order of 5 mmol N m^{-3}, and with a euphotic zone depth of 100 m, this is roughly 0.5 moles of N m^{-2} yr^{-1}. This nitrogen uptake, and thus the derived Mn uptake, is similar in magnitude to that estimated based on the primary production from Michel et al. (2006).

Text S4. Calculation of Net Mn transport through Parry Channel.

In this study, we calculated net Mn transport from Canada Basin into Parry Channel and from Parry Channel into Baffin Bay via Lancaster Sound. The boundaries are defined along lines of constant i or j indices (Fig. S14). The Mn flux across each of the boundaries, ϕ_{bdy}, is the sum of the dissolved Mn concentration at the boundary grid points with indices i, j, k, multiplied by the volume flux:

$$\phi_{bdy}(t) = \sum_{i,j,k} [dMn]_{i,j,k}(t) \cdot u_{i,j,k}(t) \cdot A_{i,j,k} \tag{8}$$

where u is the velocity perpendicular to the boundary at time, t, and A is the grid cell area. These time series were calculated from 5-day modelled velocity and tracer fields, interpolated onto the U grid.

Mn transport into and out of Parry Channel fluctuates seasonally, with a peak in the late summer (Fig. S17). The flux of Mn in the "clean" sea ice experiment is consistently smaller than for the experiment with sediment in sea ice. To compare the experiments, we calculate the percent contribution of the sea ice component to the net transport:

$$p = (1 - \frac{\phi_{off}}{\phi_{on}}) \cdot 100\% \tag{9}$$

where ϕ_{off} is the Mn transport from an experiment with the component "off", i.e. the "clean" sea ice experiment, and ϕ_{on} is the Mn transport from an experiment with the component on, i.e. the reference experiment with dirty sea ice. Based on these calculations, the sediment released by sea ice contributes about 87% to the Mn transported from Canada Basin into Parry Channel and about 34% for the Mn transported from Parry Channel into Baffin Bay (Fig. S18). The sea ice contribution to Mn flux does not vary significantly between 2002-2019.

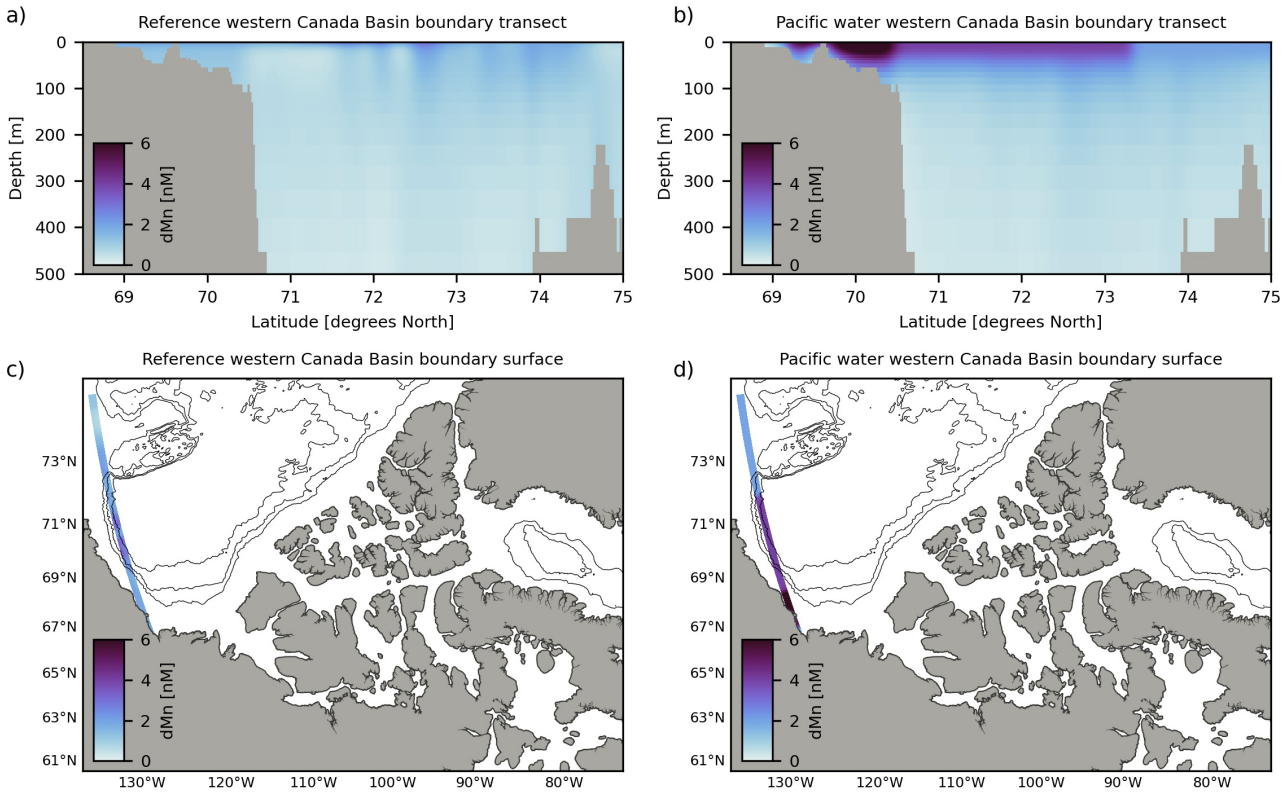

Figure S1. Western boundary conditions for dissolved Mn concentrations in the reference experiment (a, c) and Pacific water experiment (b, d). Panels (a) and (b) are vertical cross-sections of dMn concentrations along the boundary and (c) and (d) are plan views of surface dMn concentrations. The western boundary in our model domain extends from the Beaufort Sea along the shelf towards the central Arctic Ocean (Fig. 1). Pacific origin water is transported by the Alaskan Coastal Current along this shelf and enters our domain through the western boundary. The reference experiment boundary conditions (a, c) are based on the Mn model from Van Hulten et al. (2017) and are lower than observations in this region. In the Pacific water experiment (b, d), we artificially enhanced Mn concentrations along the shelf in the western boundary.

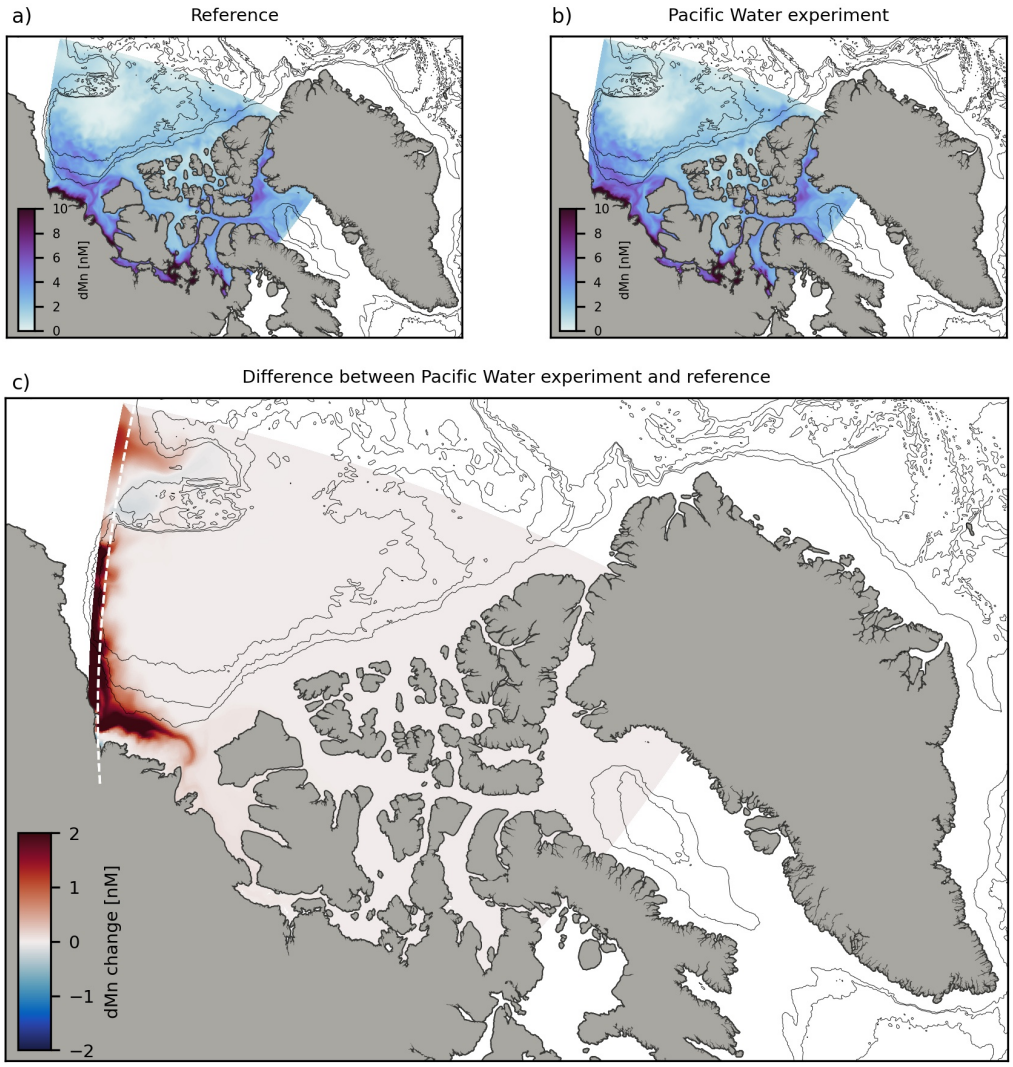

Figure S2. Depth-weighted mean dissolved Mn concentrations in the polar mixed layer in September, 2005 for the reference experiment (a), the Pacific water experiment (b), and the difference between them (c). In the reference experiment, the western boundary condition concentrations are based on the Mn model from Van Hulten et al. (2017), while we artificially enhanced concentrations along the shelf in the Pacific water experiment (Text S1, Fig. S1). Pacific origin water is transported by the Alaskan Coastal Current and its impact on dissolved Mn concentrations in the polar mixed layer is constrained to the Beaufort Shelf and does not significantly extend into the interior of the Canada Basin. The white dashed line indicates the inner-edge of the boundary condition and thin black lines correspond to bathymetry contours of 1000, 2000, and 3000 m depth.

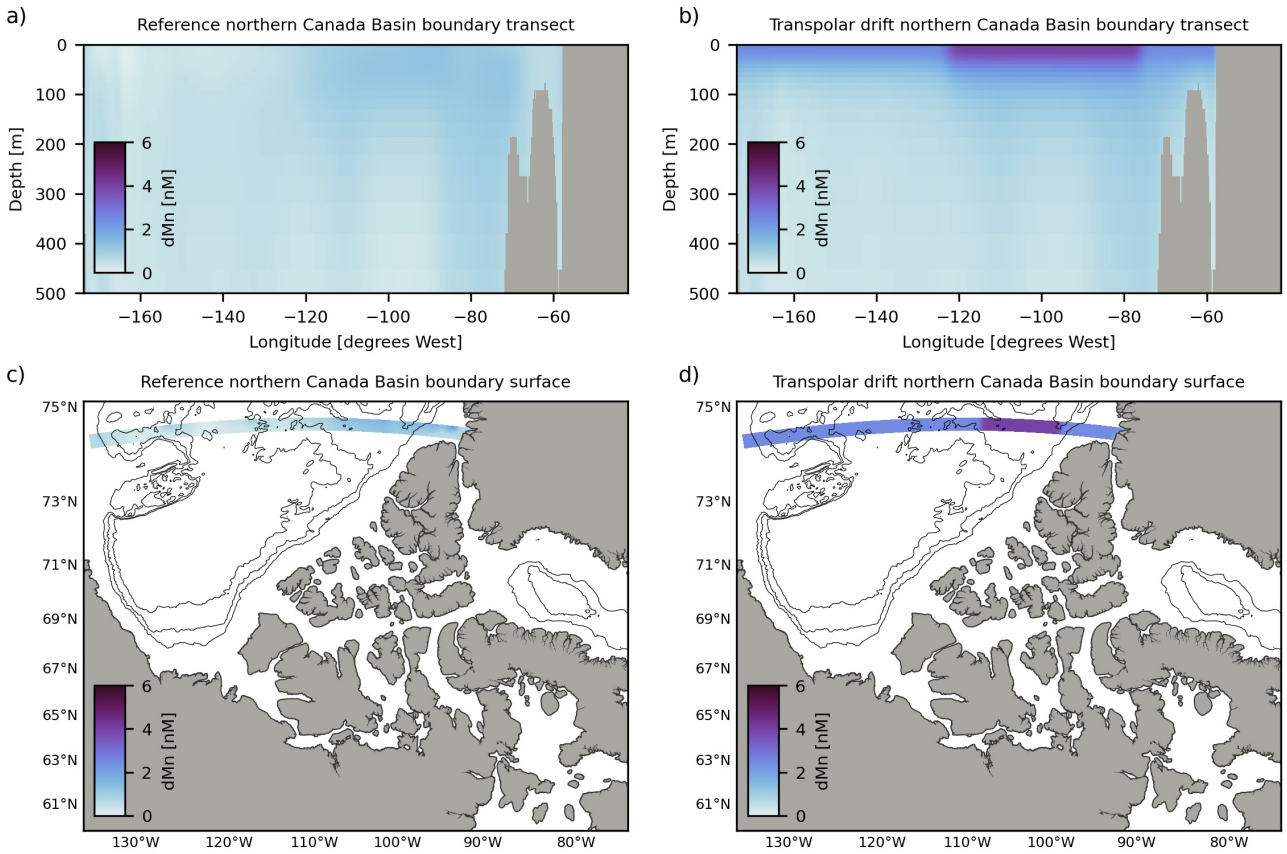

Figure S3. Northern boundary conditions for dissolved Mn concentrations in the reference experiment (a, c) and the transpolar drift experiment (b, d). Panels (a) and (b) are vertical cross-sections of dMn concentrations along the boundary and (c) and (d) are plan views of surface dMn concentrations. The northern boundary in our model domain extends across the central Arctic Ocean to Greenland (Fig. 1). The reference experiment boundary conditions (a, c) are based on the Mn model from Van Hulten et al. (2017) and are lower than observations in this region. In the transpolar drift experiment (b, d), we artificially enhanced concentrations along the northern boundary, in particular in the region of inflow from the transpolar drift.

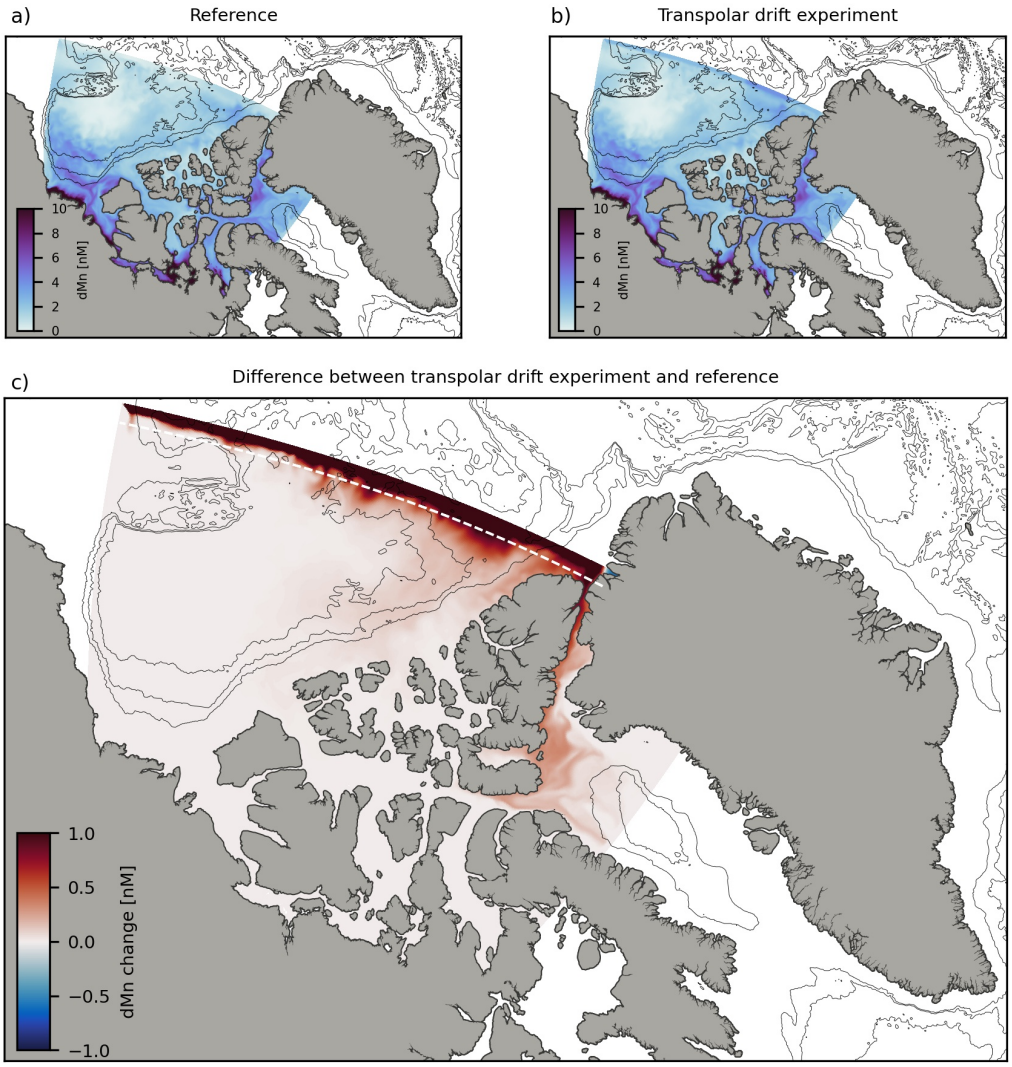

Figure S4. Depth-weighted mean dissolved Mn concentrations in the polar mixed layer in September, 2005 for the reference experiment (a), the transpolar drift experiment (b), and the difference between them (c). In the reference experiment, the northern boundary condition concentrations are based on the Mn model from Van Hulten et al. (2017), while we artificially enhanced concentrations by 2-3 nM in the transpolar drift experiment (Text S1, Fig. S3). Water from the central Arctic Ocean, including the transpolar drift, enters the Canada Basin through the northern model boundary. Near the northern boundary, dMn concentrations increased by around 0.4 nM, while concentrations increased by less than 0.1 nM in the interior of the Canada Basin. The white dashed line indicates the inner-edge of the boundary and thin black lines correspond to bathymetry contours of 1000, 2000, and 3000 m depth.

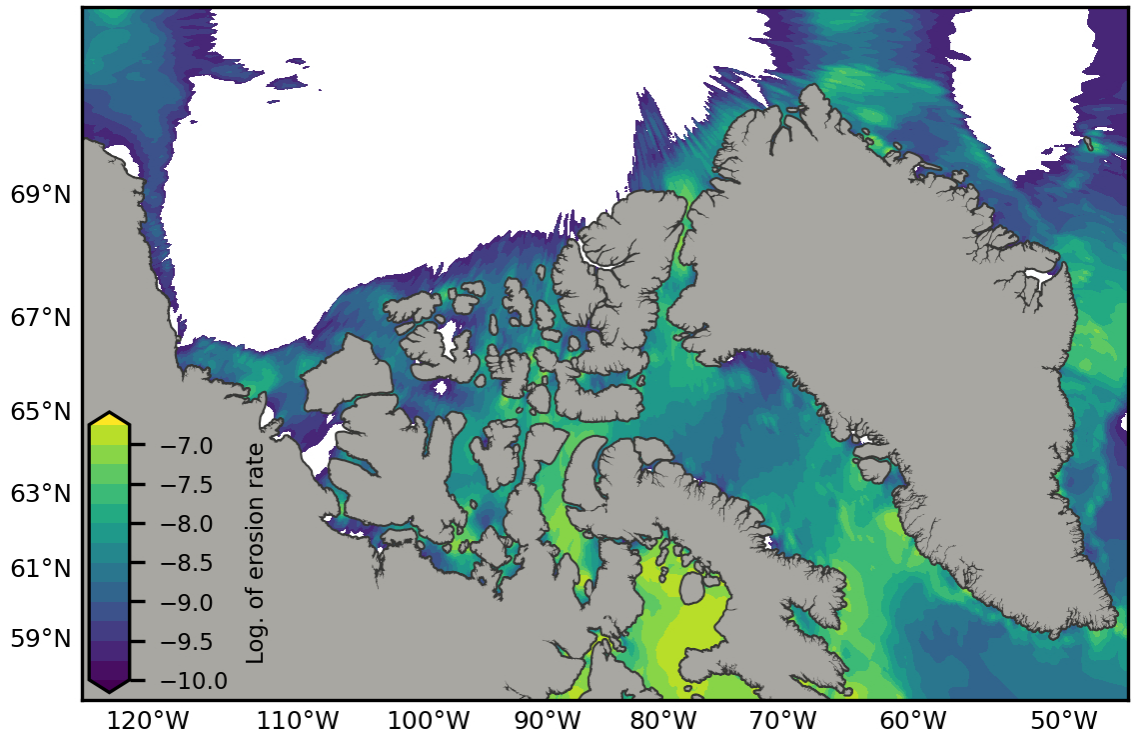

Figure S5. Erosion rates (units of kg m^{-2} s^{-1}) are heterogeneous across the Canadian Arctic. Regions west of Barrow Sill in central Parry Channel have lower erosion rates than eastern Parry Channel, as seen in observations (Colombo et al., 2020). We use tidal stress to estimate the spatially variable erosion rate for the sediment resuspension parameterization of our Mn model (Eqn. 6). Tidal stress is calculated as the squared barotropic tidal speeds derived from the MOG2D-G model (Carrère & Lyard, 2003). Erosion rate is zero (white) in regions where tidal speeds are below 1 cm s^{-1}. Note that the colorbar scale is logarithmic.

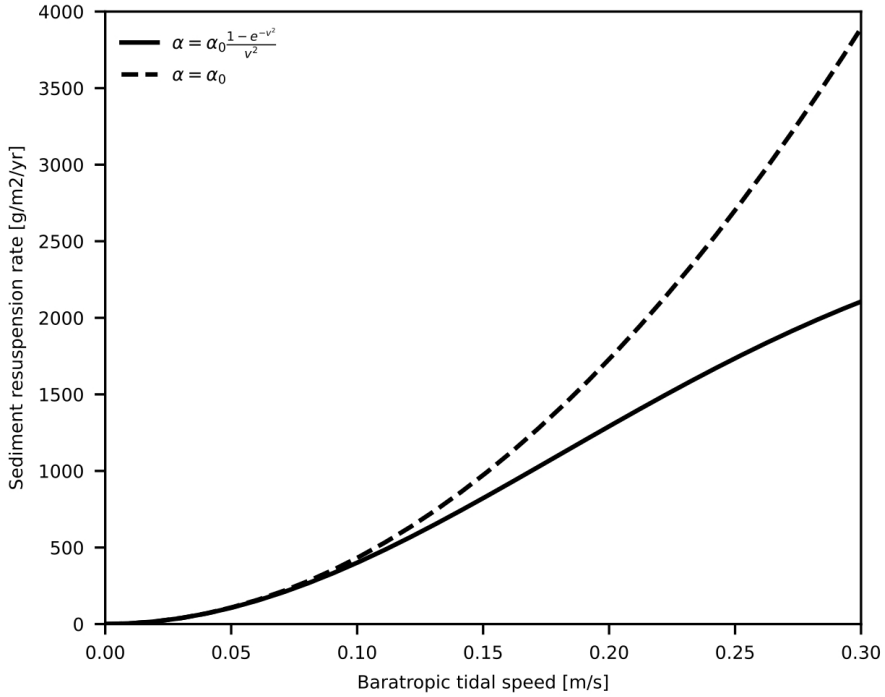

Figure S6. Sediment resuspension is modelled proportional to tidal stress (barotropic tidal speed, U_{tidal}, squared; Eqn. 5 and 6). In regions with strong tidal speeds, the readily available Mn has been dissolved from particles, and the fractional solubility is effectively reduced. We modulate the sediment resuspension rate by the fractional solubility, α, which decreases as tidal speed increases (Eqn. 7). The resulting sediment resuspension rate levels off at a maximum value at high tidal speeds (solid line), while with a constant fractional solubility, sediment resuspension increases indefinitely (dashed line).

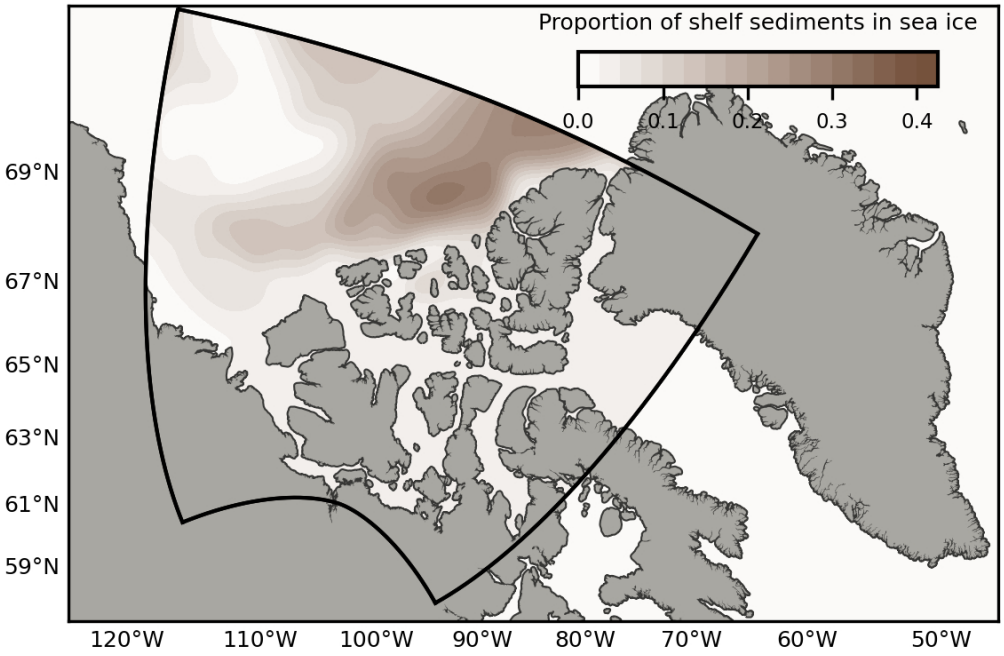

Figure S7. The sediment content of sea ice is highest along the outer edges of the Canada Basin, while the older sea ice at the core of the Beaufort Gyre is relatively "clean" in our model forcing field. The parameterization for sediment content in sea ice consists of a constant characteristic shelf sediment density, multiplied by the proportion of Siberian shelf-origin sediments in sea ice (colored contours in figure), estimated with backwards particle tracking. Within the CAA, we assume a constant, low background content.

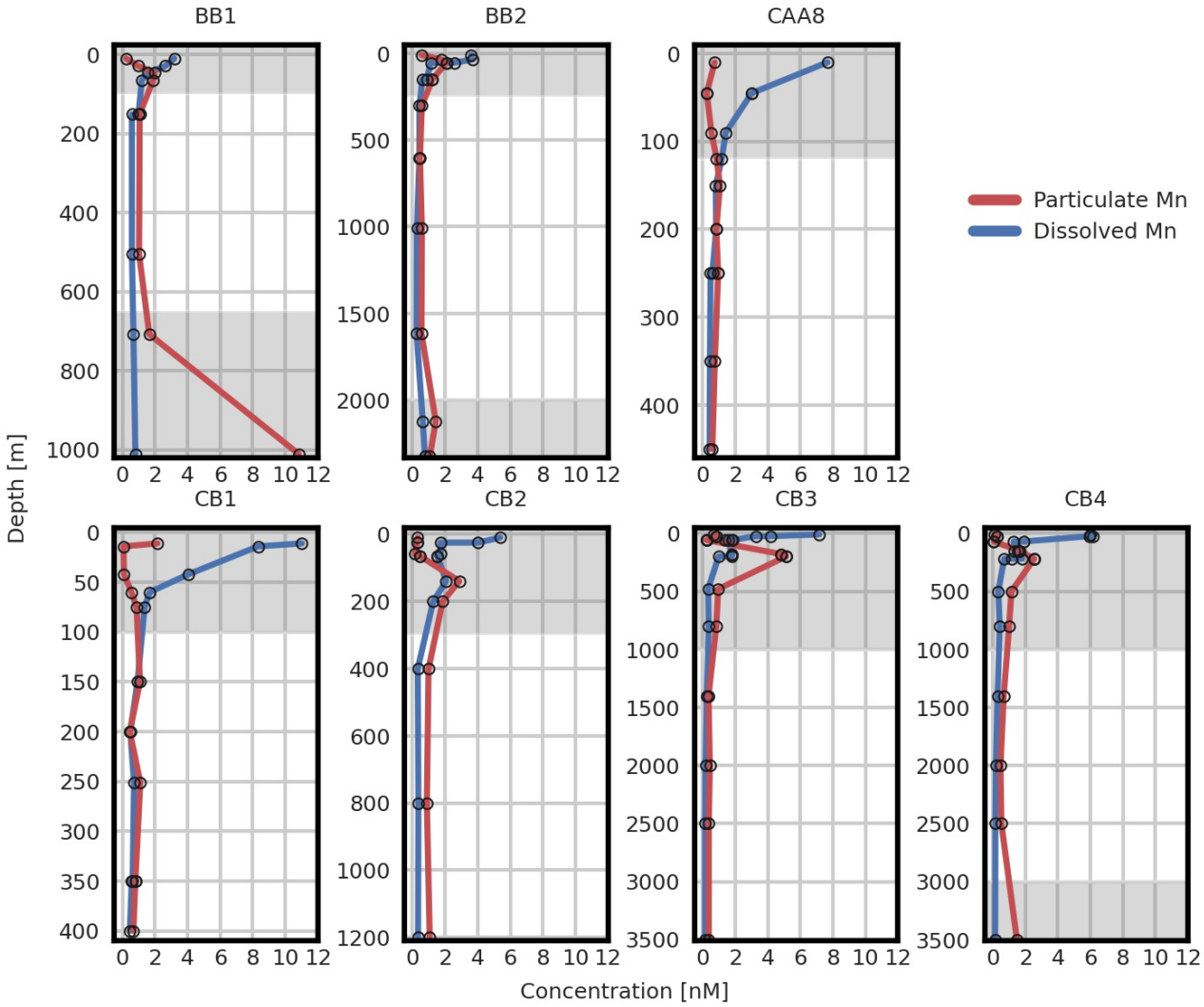

Figure S8. Scavenging rates are estimated using dissolved and particulate Mn observations far away from sources and sinks, and at depths with a negligible vertical gradient in particulate concentrations. Here, we show profiles of dissolved Mn (blue) and particulate Mn (red) from 2015 at stations in Baffin Bay, the Canadian Arctic Archipelago, and Canada Basin, that match these criteria. The depths at which external sources affect the Mn concentrations are highlighted in gray and are excluded from the scavenging rate estimate. Note that the depth scale varies between plots.

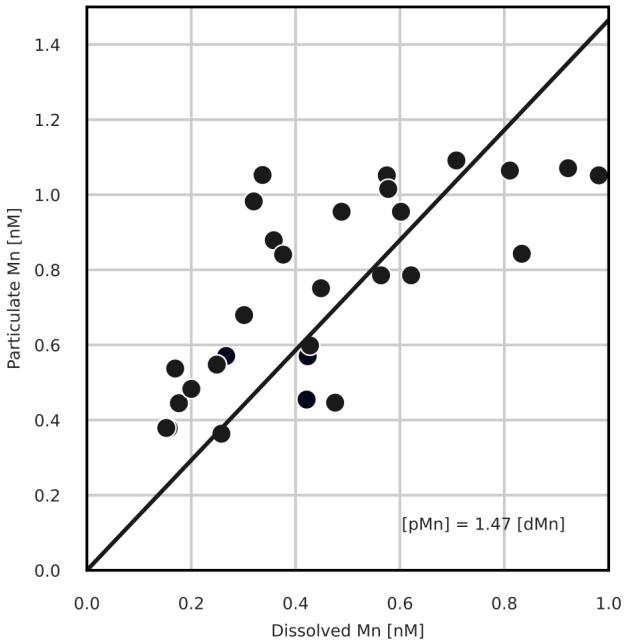

Figure S9. Far away from sources and sinks, dissolved and particulate Mn occur at ratios set by the scavenging rates. We estimate the scavenging rates from 2015 Canadian GEOTRACES observations that satisfy these criteria (profiles shown in Fig. S8) by applying a linear fit with a zero intercept (solid black line); the slope is 1.47 ± 0.25 [dMn] $[\mathrm{pMn}]^{-1} = k_{de}\ (k_{ad})^{-1}$ (Eqn. S5).

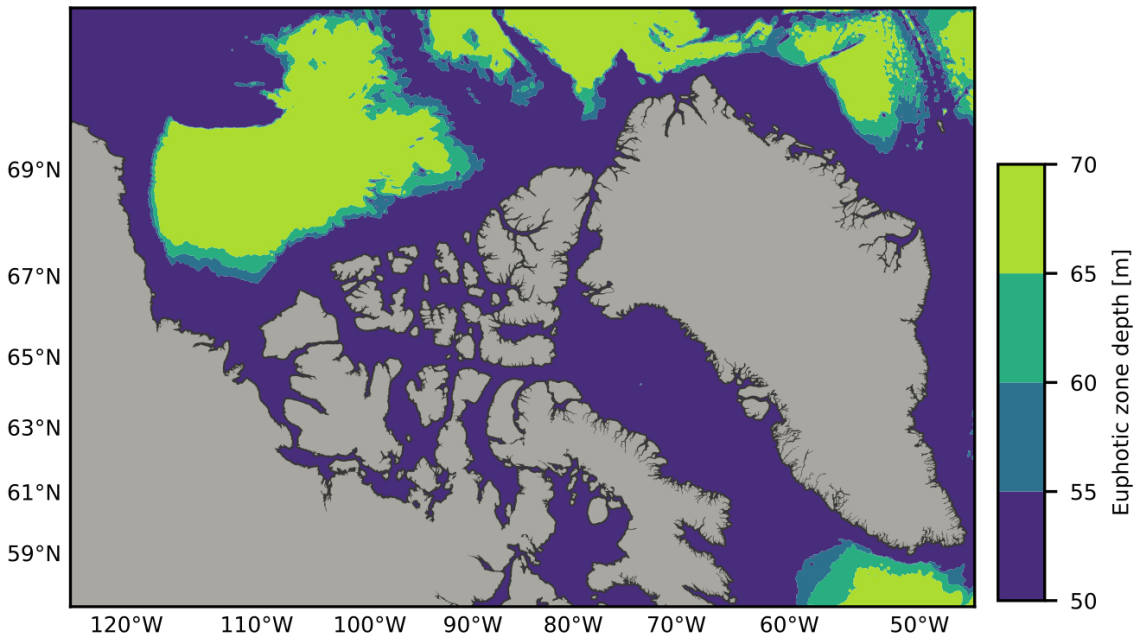

Figure S10. The euphotic zone forcing in our model gradually transitions from 70 m in the Canada Basin (shallow limit observed by Laney et al., 2017) to 50 m in the CAA based on bathymetry depth (euphotic depth from Bhatia et al., 2021). Photo-enhanced reduction is applied within the euphotic zone.

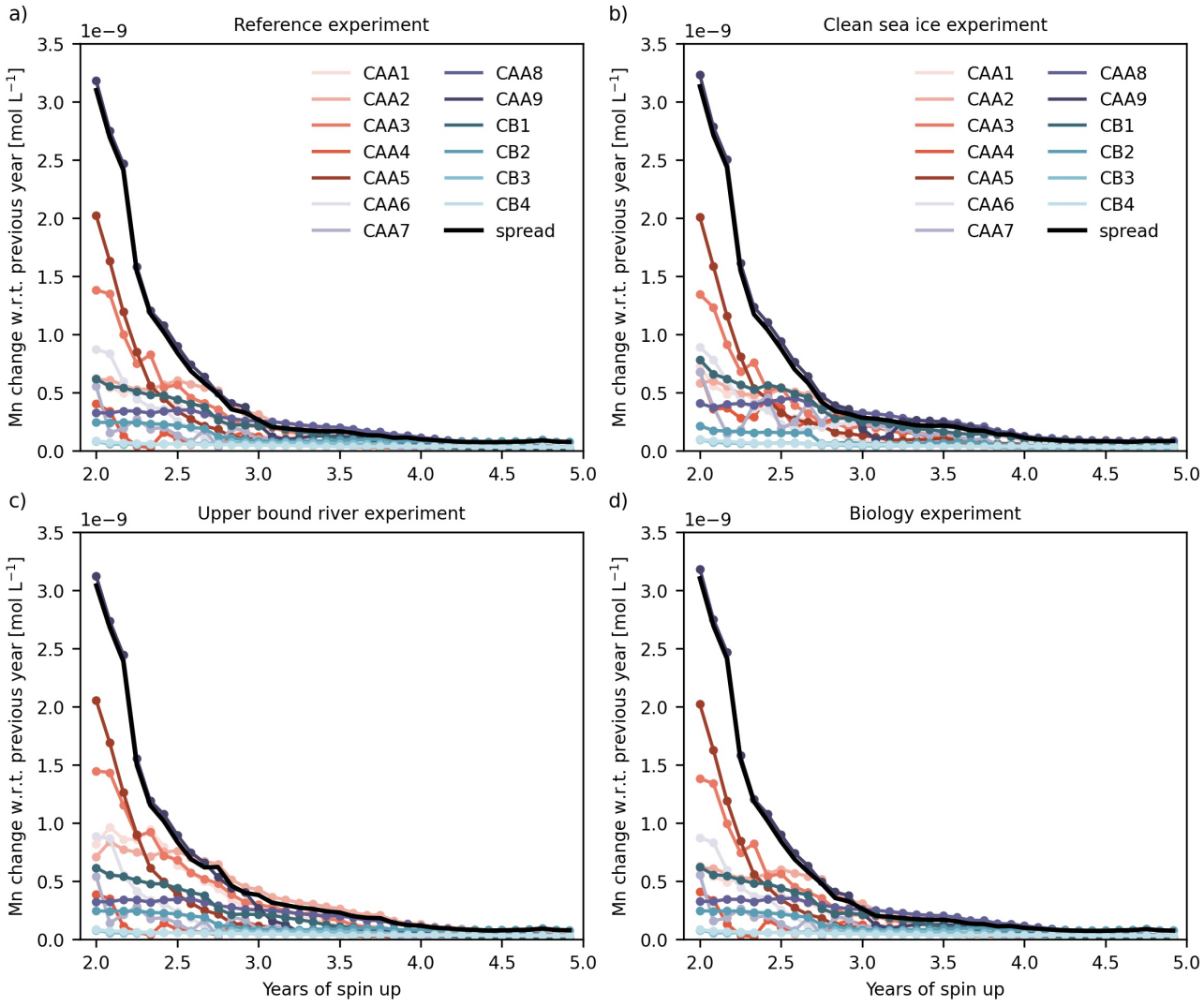

Figure S11. For each simulation: (a) reference, (b) "clean" sea ice, (c) upper bound river, and (d) biology, the Mn model is spun up by repeating the year 2002 until the year-to-year change in profile shape, estimated as the average Mn difference in the water column, at evaluation stations from 2015 Canadian GEOTRACES cruises (names in legend) is minimal. It takes about three years to achieve spin-up, after which the full experiments from 2002 to 2019 start. The "spread" is the difference between the maximum and minimum change at each month (solid black line).

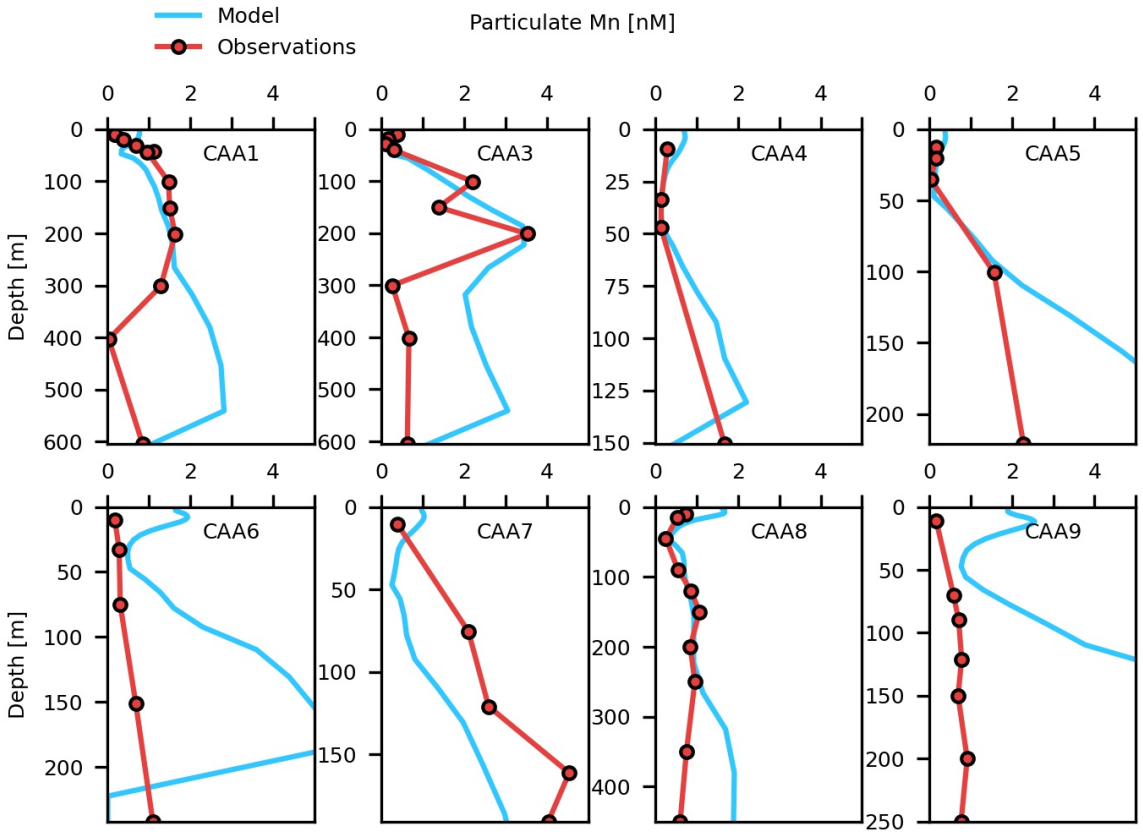

Figure S12. Modelled oxidised Mn (blue) and observed particulate Mn (red) profiles in the Canadian Arctic Archipelago for 2015 Canadian GEOTRACES stations. Observed pMn data are from Colombo et al. (2021). Particulate Mn sources are not directly incorporated into the model; instead, we modelled oMn through the coupling of scavenging with dMn. The model captures a range of behaviour within the upper 100 m of stations CAA1, CAA3, CAA4, CAA5, and CAA8, while it typically overestimates oMn in the lower water column in locations with strong sediment resuspension.

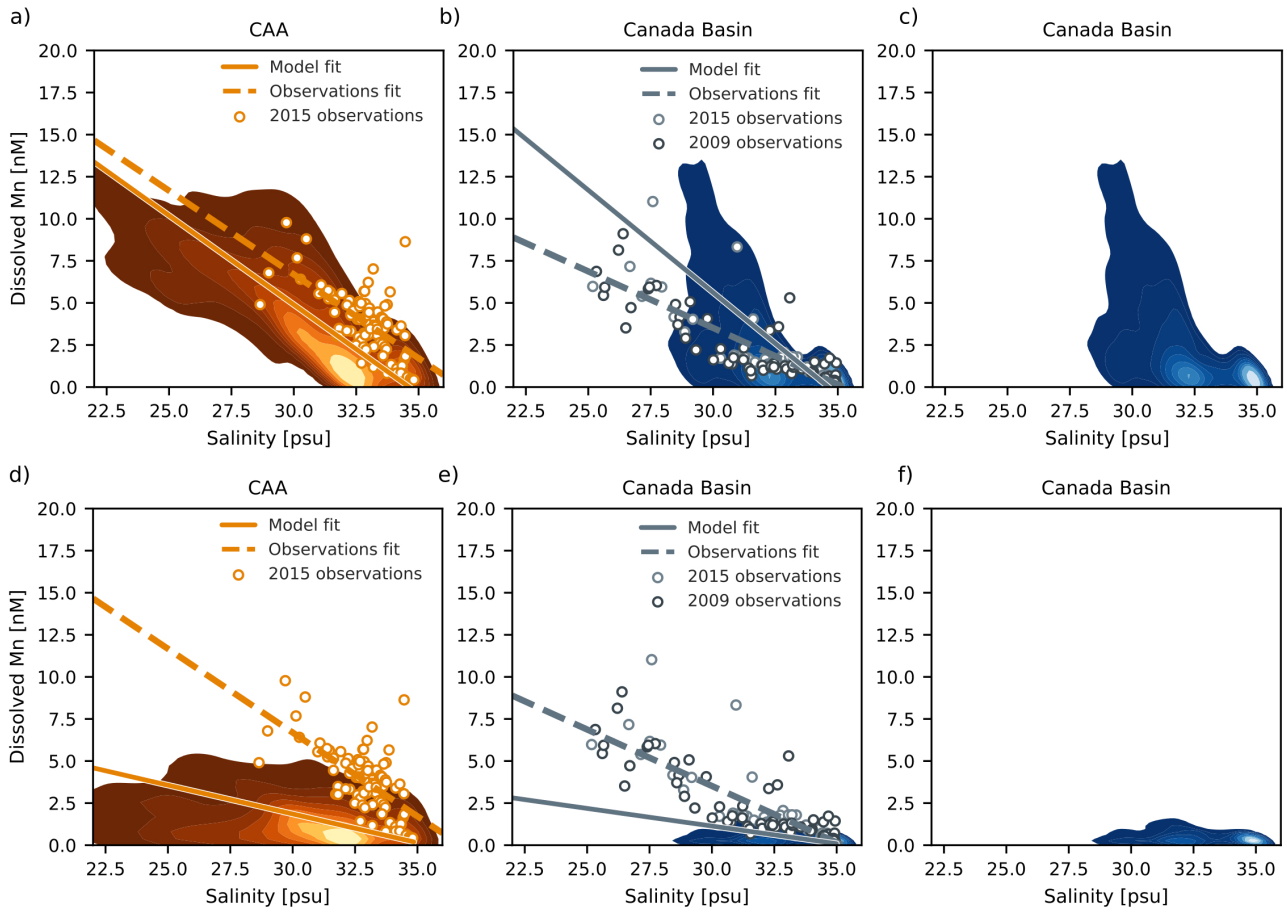

Figure S13. Modelled Mn-salinity relationship for one in five grid points at all depths (contour levels correspond to iso-proportions of the density of points) averaged over August-September, 2015, in the Canada Basin and the Canadian Arctic Archipelago (CAA) alongside observations from 2009 and 2015 (scatter points). The reference experiment (panels a-c) represents the low-salinity endmember more accurately than the experiment without sediment in sea ice (panels d-f). The solid lines are linear regression fits for the model estimates. The dashed lines are fits from observations collected in 2009 and 2015 (Sim, 2018; Colombo et al., 2020). Panels (c) and (f) show the Canada Basin contour levels alone for clarity. Note that the evaluation of the Canada Basin Mn-salinity relationship is complicated by an underestimation of surface freshwater in the model (see section 4.3.1 for a discussion of this limitation).

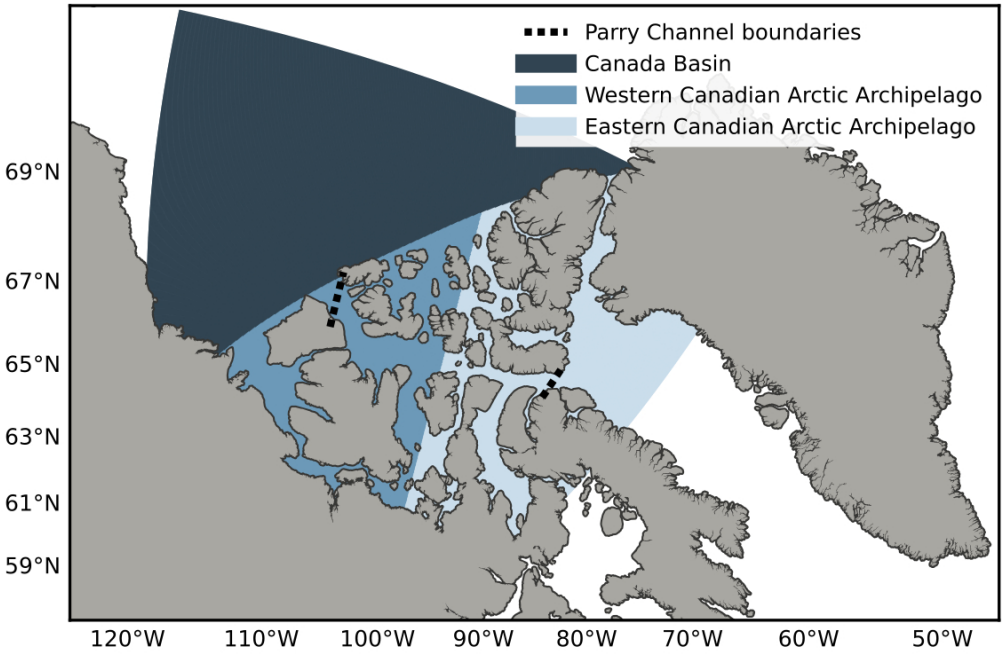

Figure S14. Region definitions for the component contribution calculations in Tables 2, 3, and S2. The CAA is divided into west and east approximately along 100°W. The boundaries indicated by black dashed lines were used for the calculations of net Mn transport into and of Parry Channel in Fig. S17 and S18.

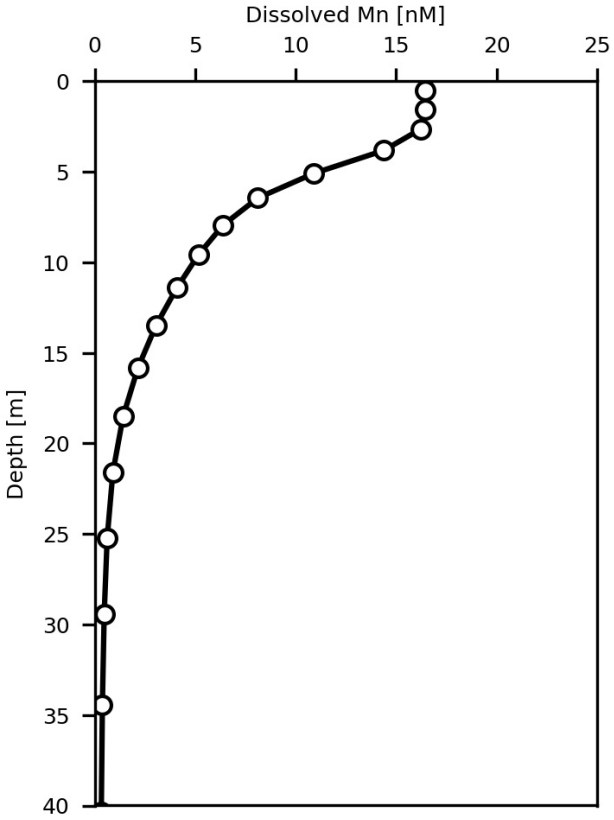

Figure S15. Dissolved Mn concentrations are highest at the surface and decrease strongly within the upper 5 m. These gradients are most visible during periods of strong surface source input, i.e. during sea ice melt. This mean profile was calculated over a sub-region of the Canada Basin (dashed white line in Fig. S16) for July, 2015. The markers indicate the model depth levels.

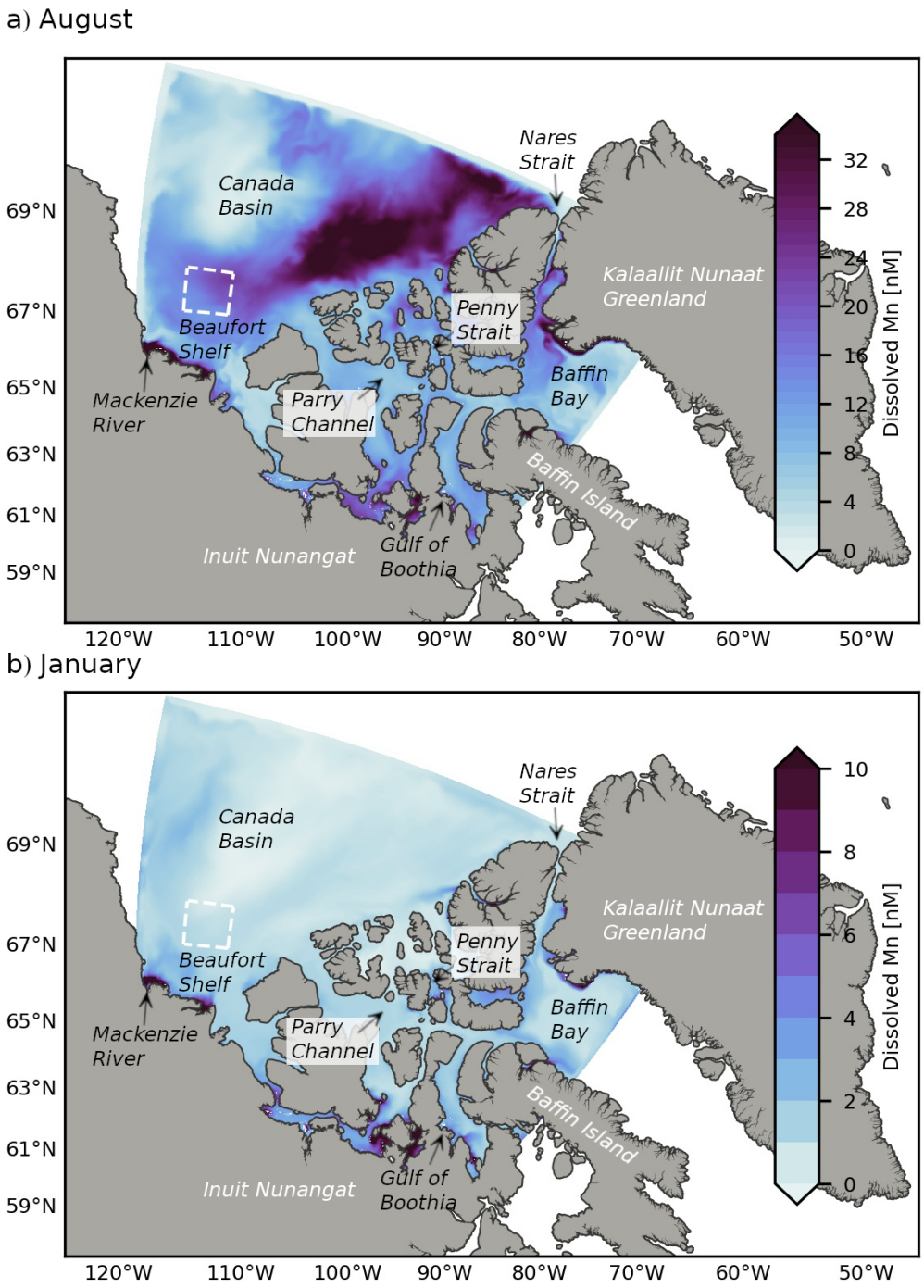

Figure S16. Simulated Mn concentrations in the ocean surface (top 1 m) in (a) August, 2015 and (b) January, 2015. The region outlined by a white dashed line is used to calculate a mean Mn profile with depth (Fig. S15). Note that the surface concentrations are much higher than for the polar mixed layer fields presented in Fig. 9, since there is a strong surface Mn gradient (as shown in Fig. S15). Panel (a) and (b) have different colorbar scale ranges.

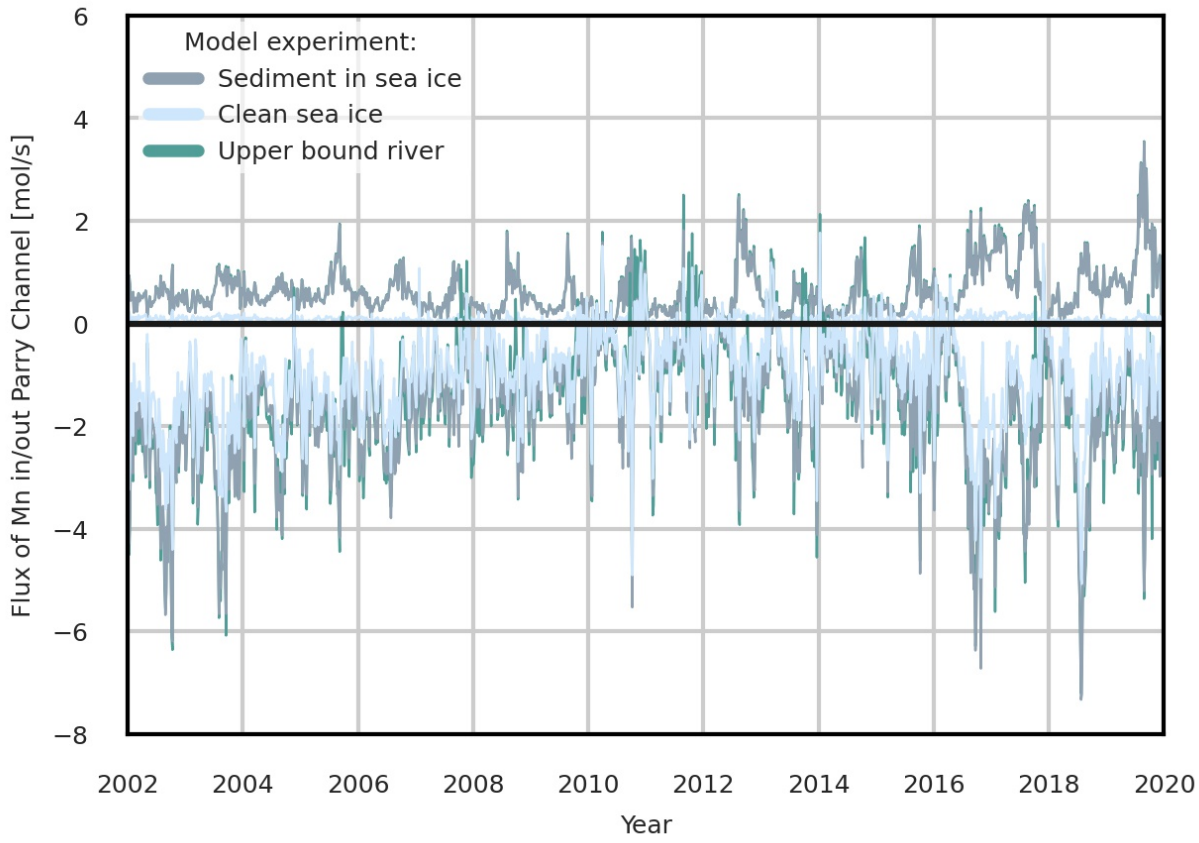

Figure S17. Mn flux into and out of Parry Channel along the boundaries defined in Fig. S14 for each of the main model experiments (calculation described in Text S4). The experiment with sediment in sea ice is the "reference" and uses a lower bound river estimate which incorporates only the direct dissolved Mn contribution. The clean sea ice experiment does not include sediment in ice. The upper bound river experiment has sediment in ice and incorporates the additional contribution of suspended matter from rivers. A positive flux represents transport into Parry Channel (typically from the Canada Basin) while a negative flux is transport out of Parry Channel (towards Baffin Bay). Mn transport into and out of Parry Channel fluctuates seasonally, with a peak in the late summer.

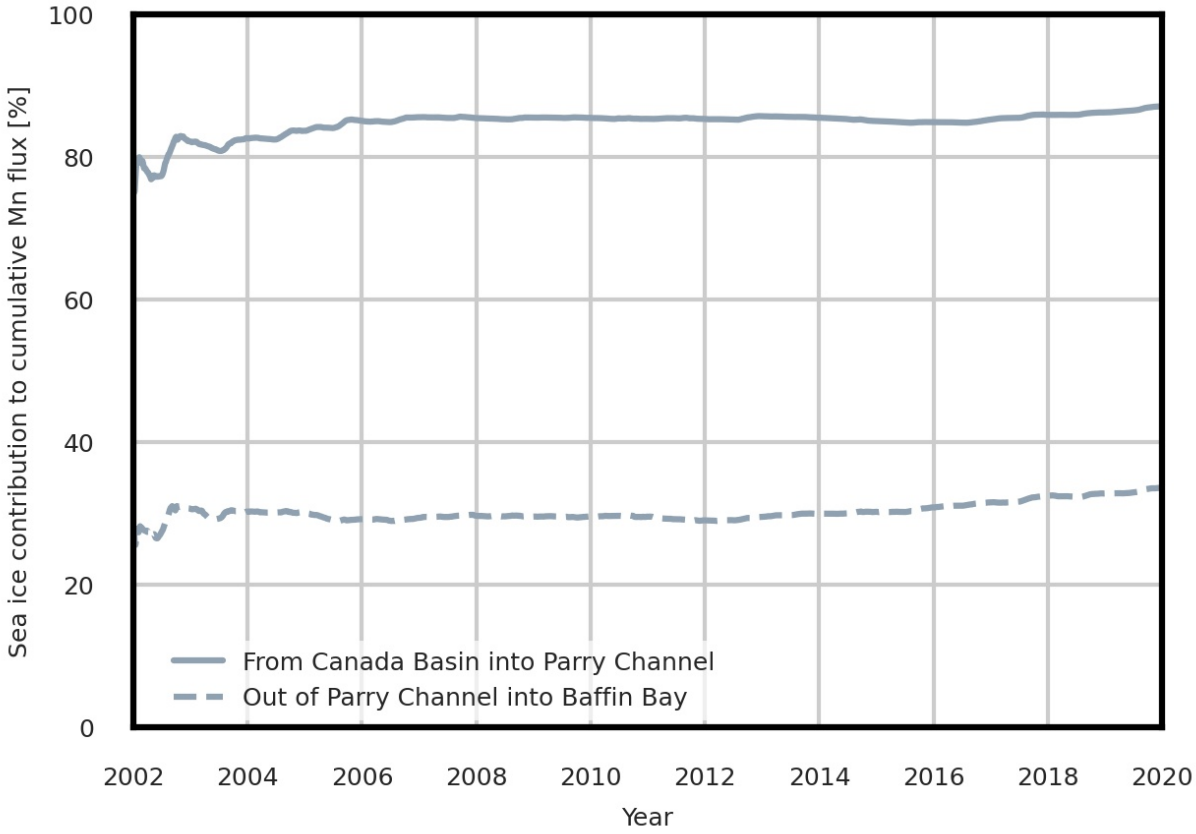

Figure S18. The percent contribution of sea ice melt to cumulative transport of Mn into and out of Parry Channel (boundaries shown in Fig. S14), estimated from the relative difference in transport between the clean sea ice and reference experiments (calculation described in Text S4). Almost 87% of Mn flowing into Parry Channel comes from sea ice melt, while it comprises about 34% of the outflow.

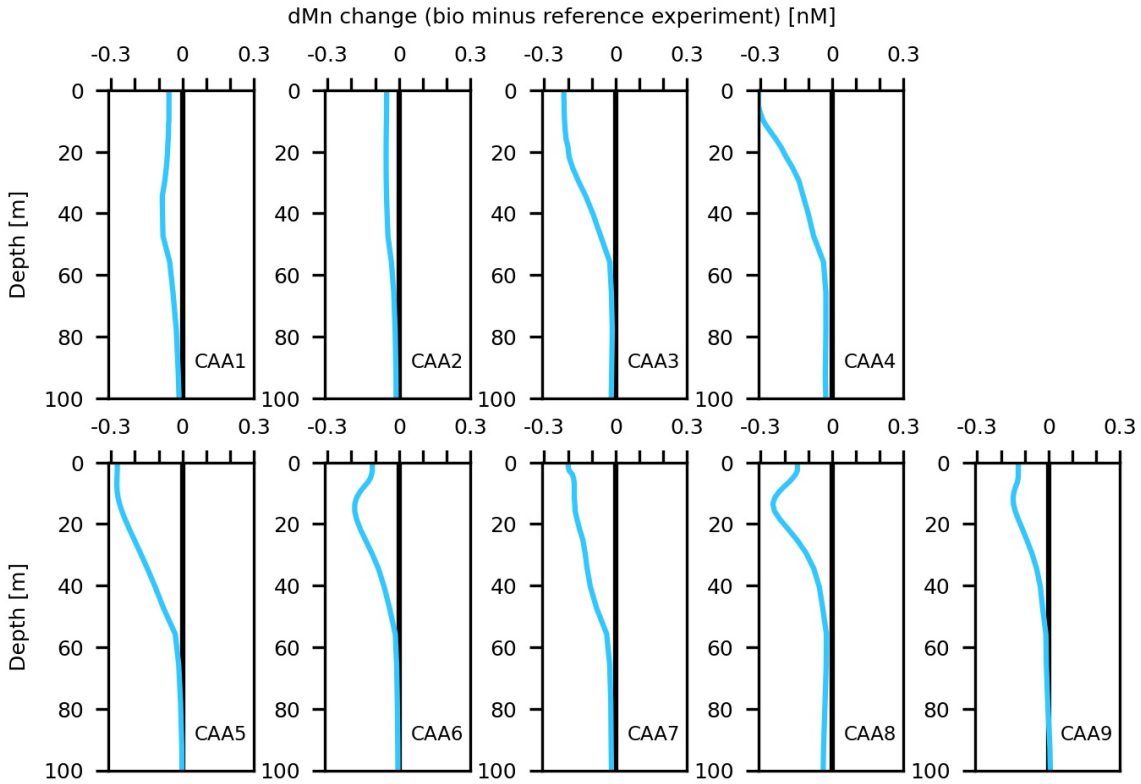

Figure S19. Difference in dissolved Mn from August-September 2015 in the upper 100 m of the water column between the experiment with uptake and remineralization of Mn ("bio" experiment) and the reference experiment for stations in the Canadian Arctic Archipelago. Uptake within the euphotic zone accounts for a reduction of up to 0.3 nM in dissolved Mn concentrations. Remineralization does not clearly appear in this figure because it occurs deeper and over a broad range of depths, and because of our coarse method of estimation using nitrate. The estimate of the magnitude of nitrate uptake is comparable to an estimate based on primary production from Michel et al. (2006) (Text S3).

Table S1. A summary of average sediment loads and suspended particulate matter (SPM) concentrations measured in sea ice cores in the Arctic Ocean. The range of measured values are in parentheses. Observed sediment content in sea ice is highly heterogeneous and can span multiple orders of magnitude. Where two estimates are given for the average content, the lower number is from "clean" ice cores and the higher number from turbid ice.

Sediment load (g m^{-2})	SPM (g m^{-3})	Location	Source
179 (0-972)	142 (24-192)	Laptev Sea	Eicken et al. (2000)
-	149 (5-500+)	Lena delta	Hölemann, Wegener, and Schirmacher (1999)
16 (9-46)	70 (8-600+)	Laptev sea	Eicken et al. (1997)
-	45, 349 (0-964)	Laptev Sea	Nürnberg et al. (1994)
(0-7000+)	-	NW of Alaska	Darby, Myers, Jakobsson, and Rigor (2011)
128 (69-203)	342 (91-508)	Chukchi Sea	Eicken et al. (2005)
232 (2-384)	564 (24-1474)	Alaska coast	Stierle and Eicken (2002)
289	157 (31-593)	Beaufort Sea	Reimnitz, Mccormick, Mcdougall, and Brouwers (1993)
1400	-	Central Arctic	Darby et al. (2011)
32 (8-84)	360 (7-2228)	Central Arctic	Tucker, Gow, Meese, Bosworth, and Reimnitz (1999)
-	68, 6800 (1-31013)	Central Arctic	Nürnberg et al. (1994)
-	24 (0-725)	Fram Strait	Dethleff and Kuhlmann (2010)
-	11 (2-137)	Kara Sea	Dethleff and Kuhlmann (2009)

Table S2. The spatial average annual dissolved Mn contributed by external model source components for the full water column (μmol m^{-2} yr^{-1}) in the reference experiment, averaged over the years 2002-2019, separated by region (Fig. S14). Sediment release by sea ice is the only component that varies significantly year-to-year. Estimates from the upper bound river experiment are indicated in parentheses.

	Canada Basin		Canadian Arctic Archipelago	
Component contribution	μmol m^{-2} yr^{-1}	%	μmol m^{-2} yr^{-1}	%
River discharge	5.3 (22)	2.1 (7.8)	19 (178)	2.3 (18)
Sediment resuspension	34	13 (12)	662	81 (68)
Sediment from sea ice	221	85 (80)	138	17 (14)
Dust released by sea ice	0.2	0.1	0.3	0.0
Direct dust deposition	0.0	0.0	0.0	0.0
Total	261 (277)	100	819 (978)	100

References

Bhatia, M. P., Waterman, S., Burgess, D. O., Williams, P. L., Bundy, R. M., Mellett, T., ... Bertrand, E. M. (2021). Glaciers and Nutrients in the Canadian Arctic Archipelago Marine System. *Global Biogeochemical Cycles*, *35*, e2021GB006976. doi: 10.1029/2021GB006976

Carrère, L., & Lyard, F. (2003). Modeling the barotropic response of the global ocean to atmospheric wind and pressure forcing-comparisons with observations. *Geophysical Research Letters*, *30*(6). doi: 10.1029/2002GL016473

Colombo, M., Jackson, S. L., Cullen, J. T., & Orians, K. J. (2020). Dissolved iron and manganese in the Canadian Arctic Ocean: on the biogeochemical processes controlling their distributions. *Geochimica et Cosmochimica Acta*, *277*, 150–174. doi: 10.1016/j.gca.2020.03.012

Colombo, M., Li, J., Rogalla, B., Allen, S. E., & Maldonado, M. T. (2022). Particulate trace element distributions along the Canadian Arctic GEOTRACES section: shelf-water interactions, advective transport and contrasting biological production. *Geochimica et Cosmochimica Acta*, *323*, 183-201.

Colombo, M., Rogalla, B., Li, J., Allen, S. E., Orians, K. J., & Maldonado, M. T. (2021). Canadian Arctic Archipelago Shelf-Ocean Interactions: A Major Iron Source to Pacific Derived Waters Transiting to the Atlantic. *Global Biogeochemical Cycles*, *35*(10), e2021GB007058. doi: 10.1029/2021GB007058

Darby, D. A., Myers, W. B., Jakobsson, M., & Rigor, I. (2011). Modern dirty sea ice characteristics and sources: The role of anchor ice. *Journal of Geophysical Research: Oceans*, *116*(9). doi: 10.1029/2010JC006675

Dethleff, D., & Kuhlmann, G. (2009). Entrainment of fine-grained surface deposits into new ice in the southwestern Kara Sea, Siberian Arctic. *Continental Shelf Research*, *29*(4), 691–701.

doi: 10.1016/j.csr.2008.11.009

Dethleff, D., & Kuhlmann, G. (2010). Fram Strait sea-ice sediment provinces based on silt and clay compositions identify Siberian Kara and Laptev seas as main source regions. *Polar Science*, *29*(3). doi: 10.3402/polar.v29i3.6070

Eicken, H., Gradinger, R., Gaylord, A., Mahoney, A., Rigor, I., & Melling, H. (2005). Sediment transport by sea ice in the Chukchi and Beaufort Seas: Increasing importance due to changing ice conditions? *Deep Sea Research Part II: Topical Studies in Oceanography*, *52*, 3281–3302. doi: 10.1016/j.dsr2.2005.10.006

Eicken, H., Kolatschek, J., Freitag, J., Lindemann, F., Kassens, H., & Dmitrenko, I. (2000). A key source area and constraints on entrainment for basin-scale sediment transport by Arctic sea ice. *Geophysical Research Letters*, *27*(13), 1919–1922. doi: 10.1029/1999GL011132

Eicken, H., Reimnitz, E., Alexandrov, V., Martin, T., Kassens, H., & Viehoff, T. (1997). Sea-ice processes in the Laptev Sea and their importance for sediment export. *Continental Shelf Research*, *17*(2), 205–233. doi: 10.1016/S0278-4343(96)00024-6

Hölemann, J., Wegener, A., & Schirmacher, M. (1999). Dissolved and particulate major and trace elements in newly formed ice from the Laptev Sea (Transdrift III, October 1995). In *Land-ocean systems in the Siberian Arctic* (pp. 101–111). Springer Berlin Heidelberg. doi: 10.1007/978-3-642-60134-7_11

Laney, S. R., Krishfield, R. A., & Toole, J. M. (2017, 9). The euphotic zone under Arctic Ocean sea ice: Vertical extents and seasonal trends. *Limnology and Oceanography*, *62*, 1910-1934. doi: 10.1002/LNO.10543

Michel, C., Ingram, R. G., & Harris, L. R. (2006, 10). Variability in oceanographic and ecological processes in the canadian arctic archipelago. *Progress in Oceanography*, *71*, 379-401. doi:

10.1016/J.POCEAN.2006.09.006

Nürnberg, D., Wollenburg, I., Dethleff, D., Eicken, H., Kassens, H., Letzig, T., & Reimnitz, E. (1994). Sediments in Arctic sea ice: Implications for entrainment, transport and release. *Marine Geology*, *119*, 185–214. doi: 10.1016/0025-3227(94)90181-3

Reimnitz, E., Mccormick, M., Mcdougall, K., & Brouwers, E. (1993). Sediment export by ice rafting from a coastal polynya. *Arctic, Antarctic, and Alpine Research*, *25*(2), 83–98. doi: 10.1080/00040851.1993.12002988

Sim, N. (2018). *Biogeochemical cycling of dissolved and particulate manganese in the north-east Pacific and Canadian western Arctic* (Doctoral dissertation, University of British Columbia). doi: 10.14288/1.0374222

Stierle, A. P., & Eicken, H. (2002). Sediment inclusions in Alaskan coastal sea ice: Spatial distribution, interannual variability, and entrainment requirements. *Arctic, Antarctic, and Alpine Research*, *34*(4), 465–476. doi: 10.1080/15230430.2002.12003518

Tucker, W. B., Gow, A. J., Meese, D. A., Bosworth, H. W., & Reimnitz, E. (1999). Physical characteristics of summer sea ice across the Arctic Ocean. *Journal of Geophysical Research: Oceans*, *104*(C1), 1489–1504. doi: 10.1029/98jc02607

Van Hulten, M., Middag, R., Dutay, J.-C., De Baar, H., Roy-Barman, M., Gehlen, M., ... Sterl, A. (2017). Manganese in the west Atlantic Ocean in the context of the first global ocean circulation model of manganese. *Biogeosciences*, *14*, 1123–1152. doi: 10.5194/bg-14-1123-2017